Fabrication of nanostructured MgO:Fe as NO₂ gas sensor prepared by spray pyrolysis technique

H. R. Abd Ali[a], R. I. Jasim[b], K. N. Hussein[c], S. S. Chiad[b,*] , N. F. Habubi[d],
Y. H. Kadhim[e], M. Jadan[f,g]
[a]*Department of Physics- College of Education for Pure Sciences-University of Tikrit, Iraq*
[b]*Department of Physics, College of Education, Mustansiriyah University, Iraq*
[c]*Department of Radiology, Al-Manara College for Medical Science, Iraq*
[d]*Department of Radiology and Sonar Techniques, Alnukhba University University College, Baghdad 10013, Iraq*
[e]*Department of Optics Techniques, College of Haelth and Medical Techniques, AL-Mustaqbal University, Babylon, Hillah, 51001, Iraq.*
[f]*Department of Physics, College of Science, Imam Abdulrahman Bin Faisal University, P.O. Box 1982, 31441 Dammam, Saudi Arabia*
[g]*Basic and Applied Scientific Research Center, Imam Abdulrahman Bin Faisal University, P.O. Box 1982, 31441 Dammam, Saudi Arabia*

Nanostructured MgO:Fe was fabricated by spray Pyrolysis technique (SPT). XRD verifies MgO's cubic structure. The MgO thin film's crystallite size increased to 10.7–15.41 nm due to doping. SEM pictures display The surface becomes rougher and the grain size increases with concentration. The ideal MgO's average transmission value in the visible spectrum was 70%. The Tauc relation was used to calculate Eg, which decreased for MgO:Fe doping at 4%wt concentration from 362.1 to 3.52 eV. Resistance change as a measure of film sensitivity to gas indicates that MgO is a p-type semiconductor, with the maximum resistance being shown by MgO:Fe at 4%wt. The sensitivity of MgO films to NO₂ diminishes as Fe content increases.

1. Introduction

Magnesia, also known as MgO, is naturally available as periclase and serves as a magnesium source MgO has a wide bandgap of 7.8 eV suited for use as insulators [1,2]. Because of its optical transparency and high magnetic field, MgO is a popular semiconductor material. MgO has been intensively researched as a thin film in recent research since it is a one-of-a-kind solid with a strong ionic character and simple stoichiometry. However, using MgO thin films can improve various applications, including catalysis, ceramics, solar cells, and reflective and antireflective coatings. [3-5]. Doping inorganic materials with Fe ions seemed appealing because it permits visible energy transitions in higher and lower energy areas apart from the wide bands produced by absorption and emission processes [6]. Doping can alter the structure of MgO nanoparticles with (110) or (111) faces and can be used to stabilize them. Doping can also cause changes in the electrical characteristics of nanoparticles by promoting the creation of O vacancies or offering newly occupied states above the valence band [7]. Spray pyrolysis was employed to create transparent oxide coatings as early as 1910 [8]. Numerous experimental techniques have been developed to produce magnesium oxide (MgO), including PLD [9], PVD [10], CVD [11], laser ablation [12], sol-gel [13, 14], reactive sputtering [15], metal-organic MBE [16], pulsed laser deposition [17] and CSP [18]. When sprayed micro-droplets reach the heated substrate surface,

---

they decompose pyrolytically and produce a single or cluster of crystallites [19]. This work aims to use the CSP method to investigate the impact of Fe on the physical features of MgO films.

2. Experimental

Thin films of MgO doped with Fe were fabricated via SPT. 0.1 M of $(Mg(CH_3COO)_2)$ was dispersed in 100 ml of deionized water to produce the precursor solution. $FeNO_3$ was utilized as the doping material to create doping concentrations of 2% and 4%, which were added to the precursor solution. The substrate temperature was 450°C during the deposition procedure, using N_2 as the carrier gas, and with a nozzle-to-base distance of 29 cm. The spraying parameters included an 8-second spraying time, a 5 mL/min spraying rate, and a gap of two minutes between two successive spray operations. The film thickness, determined gravimetrically, was approximately 325 ± 30 nm. XRD was employed to analyze the film structure, and Surface Topography has been examined via AFM. SEM of a model (multi-function scanning electron microscope model als 2300 Angstrom). Optical transmittance in the range of 300 to 900 nm was measured using a spectrophotometer. The MgO gas sensor was fabricated with aluminum electrodes on thin films, and gas sensitivity was evaluated by the resistance change percentage in a cylindrical chamber (radius: 7.5 cm, height: 15 cm).

3. Results and discussions

Fig. (1) offers XRD styles of MgO and MgO doped via Fe with (2 and 4) % wt. According to the standard JCPDS card No. (01-075-0477), the high diffraction peaks at 111 and low diffraction peaks at (200) indicate a cubic structure with polycrystalline nature. There is no indication of any other secondary phase, such as Fe or iron oxide. We discovered that with the rise in Fe concentration, the position of the peaks in the (111) direction changed to lower angle 2θ diffraction, and their β (FWHM) also shrank. The shift in peak positions and the decreased FWHM demonstrated that Fe ions had replaced Mg sites in the MgO crystal matrix. This could be due to the larger Fe2+ ions (0.78Å) replacing the smaller Mg^{2+} ions (0.72Å) [20, 22].

An alteration in the Mg–O bond length and the overall lattice parameter was observed, consistent with previous findings [23, 24].

Scherrer's formula was used to compute the average grain size (D) [25-26]:

$$D = \frac{k\lambda}{\beta cos\theta}$$ (1)

where K =0.9, λ = 1.54Å, βis (FWHM). The average particle size of pure, 2 %wt and 4 %wt of Fe doping concentration was 10.7 nm, 13.46 nm and 15.41 nm, respectively. The average particle size of Fe doped MgO increases with increasing iron content. It is well known that Fe2+ can substitute for Mg^{2+} ions in the MgO crystal lattice [27].

The dislocation density (δ) was calculated using equation (2) [28-29]:

$$\delta = \frac{1}{D^2}$$ (2)

Microstrain (ε) of the MgO nano-grains were estimated using the following equation (3) [30, 31]:

$$\varepsilon = \frac{\beta cos\theta}{4}$$ (3)

Fig. (2) illustrates the variations in crystallite size, β, strain, and dislocations as the dopant concentration increases. The observed increase in dislocation density, coupled with the reduction

in lattice strain and the generation of dislocations due to Fe doping, increases oxygen vacancies to offset the charge within the MgO lattice [32-33]. The structural parameters for the dominant (111) peak are computed and presented in Table 1.
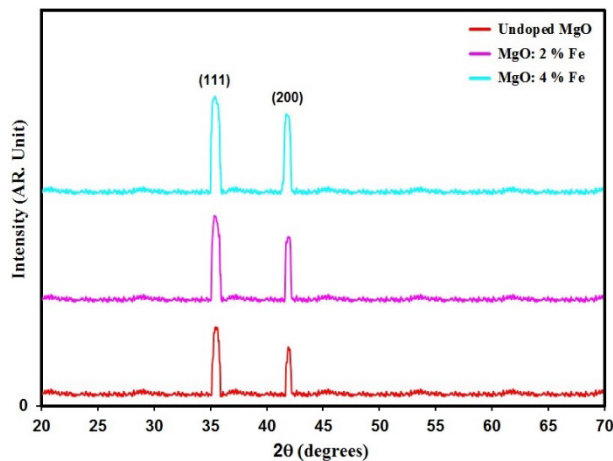

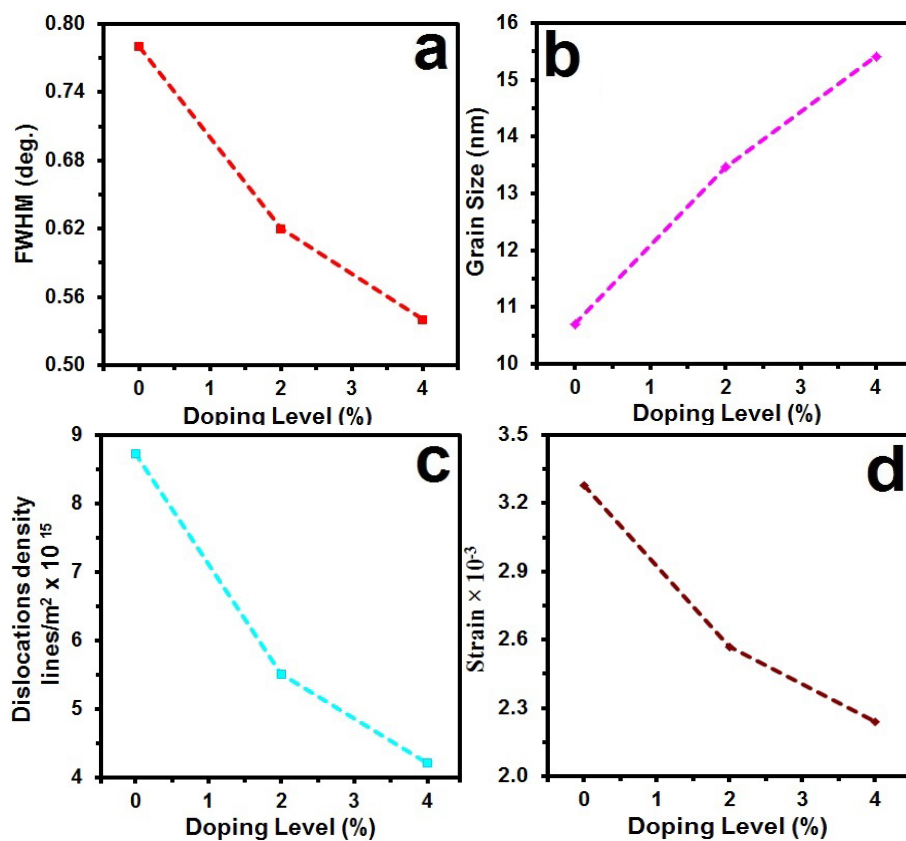*Fig. 1. Displays the XRD patterns of the desired films.*

Fig. 2. X-ray parameters of intended films.

Table 2. Provides structural parameters for the intended films.

Samples wt %	2Θ ($^{\circ}$)	(hkl) Plane	β ($^{\circ}$)	Eg (eV)	(D) (nm)	$(\delta) \times 10^{15}$ (Line. m^{-2})	$\varepsilon \times 10^{-3}$ ($Line^{-2}{\cdot}m^{-1}$)
Undoped MgO	35.82	111	0.78	3.62	10.70	8.73	3.28
MgO: 2% Fe	35.61	111	0.62	3.58	13.46	5.51	2.57
MgO: 4% Fe	34.55	111	0.54	3.52	15.41	4.21	2.24

The three-dimensional area of MgO and doped thin films with (2 and 4 % wt Fe concentrations) deposited at 450oC temperatures is shown in Fig. 2. The films are uniform, tightly packed, and pinhole-free. Table 2 demonstrates that grain diameters vary from 73.52-60.87nm as the Fe ratio concentration increases. However, Table 2 displays the surface roughness(Ra) and Root Mean Square (RMS) values. As the Fe doping ratio rises, it is evident that Ra and RMS values decrease, suggesting an increase in grain size, which is consistent with other literature [34]. Figure 3 depicts a histogram of the percentage of MgO and doping in Fe against particle size Ps.
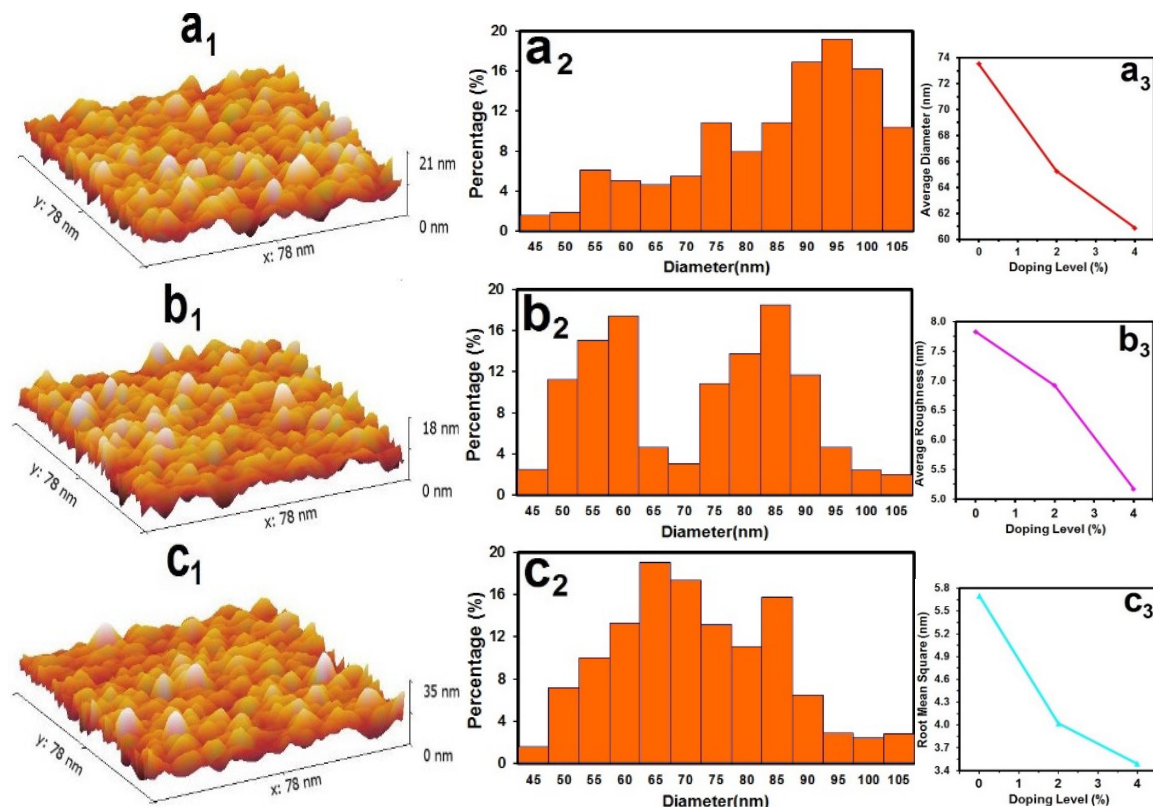

Fig. 3. Displays the AFM images of grounded films.

Table 2. Provides the AFM parameters of grown films.

Samples	P_s nm	R_a nm	RMS nm
Undoped MgO	73.52	7.83	5.70
MgO:2% Fe	65.25	6.92	4.02
MgO: 4% Fe	60.87	5.17	3.49

The scanning electron microscopy (SEM) images in Fig. (4) depict MgO and MgO:Fe films deposited at various concentrations with a thickness of 325 nm. A smooth and compact surface with an average grain size of approximately 50 nm is observed. As the concentration increases to 0%, 2%, and 4%, the average grain size rises to about 31 nm, 37nm, and 46 nm, respectively. This increase in concentration leads to a progressive enlargement of the grain size, accompanied by a roughening of the surface. that the introduction of Fe alters the film's microstructure, influencing grain size and surface morphology, with higher concentrations contributing to larger grains and increased surface roughness.
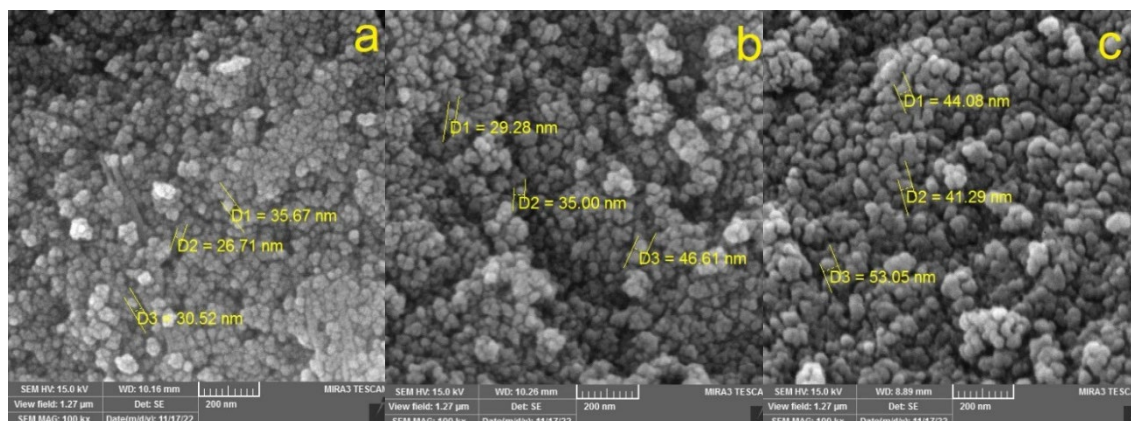

Fig .4. SEM images of MgO thin films with various Fe concentrations
(a) Undoped MgO; (b) MgO:2% Fe, (c) MgO: 4% Fe).

Experimental measurements are typically expressed in terms of the percentage transmittance (T), defined as [35, 36]:

$$T\% = \frac{I}{I_o}\%$$ (4)

where (I) is the light intensity after it passes through the sample and (I_o) is the initial light intensity. The optical transmittance (T) spectra of grown films with varied Fe concentrations (0, 2, and 4) wt% are shown in Fig. (5). We discovered that T of all samples is in the (60-70) % range. We found that the transmittance achieves a maximum in the (450-700) nm wavelength range and decreases with doping concentration. An increase in the concentration of defects at the grain boundaries may explain the observed drop in T. [37, 38].

The following equation was used to compute the absorption coefficient (α) [39, 40]:

$$\alpha = 2.303\frac{A}{t}$$ (5)

where (t) is film thickness and (A) is the absorbance. In Fig. (6) it is evident that α increases as doping concentration increases, which causes the absorption edge to be biased toward longer wavelengths. As doping increases, the density of charge atoms increases, and each electron is

1100

effectively surrounded by an exchange and correlation hole, lowering the electron's energy and shifting the conduction band to narrow [41, 42].
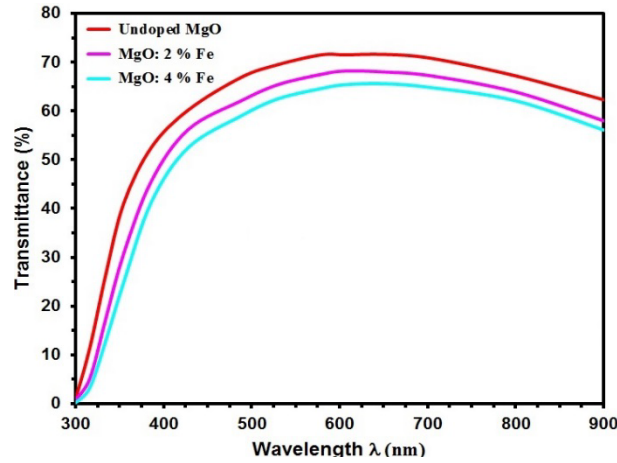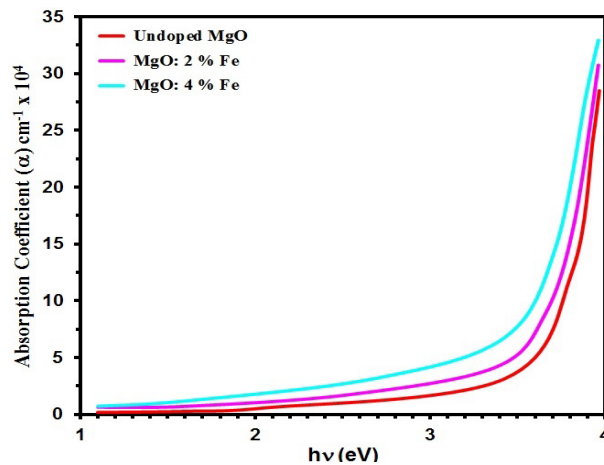

Fig. 5. Transmittance of the intended films.

Fig. 6. α for pure MgO and MgO:Fe films with different dopant levels.

Tauc formula was utilized to compute the energy gap(E_g) [43, 44]:

$$(\alpha h v) = A\left(h v - E_g\right)^{n} \tag{6}$$

where, (A) is constant, (hv) is photon energy and n = 1/2 for direct transition. The meeting point in the x-axis reflected the value of E_g, resulting in new localised levels created when MgO doping concentration was increased (donor levels). [45,46]. Fig. (7) depicts the $(\alpha h v)^2$ vs. hv for the pure and MgO:Fe films. E_g was reduced from 362.1 to 3.52 eV for MgO:Fe doping at 4%wt concentration. This reduction in E_g is attributed to Fe metal ions, which induce alterations in the optical band gap [47].
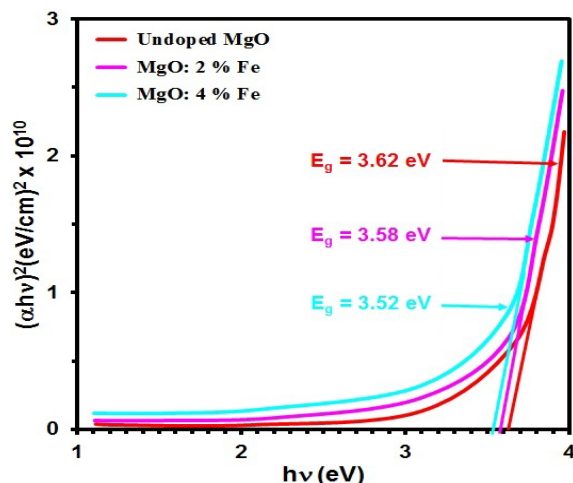
Fig. 7. Direct bandgap of grown films.

Equation 6 is employed to calculate the extinction coefficient [48]:

$$k = \frac{\alpha\lambda}{4\pi} \tag{7}$$

In general, k curves reveal a rather intense and broad absorption peak at 500 nm, as shown in Fig. (7). The VIS area has the highest value of k, which continuously increases with increasing Fe doping ratio. According to the transmittance spectra, the value of k (Fig. 8) is 0.85–0.87, suggesting high transparency film [18].

Using reflectance (R) spectra is a valuable method for determining the refractive index (n) [59, 50]:

$$R = \left(\frac{n-1}{n+1}\right)^2 \tag{8}$$

The following equation can be used to compute the refractive index (n) [51, 52].

$$n = \frac{1 + \sqrt{R}}{1 - \sqrt{R}} \tag{9}$$

The figure demonstrates that the refractive index increases as doping concentrations increase (9). In most of the visible section of the spectra, the n values of the pure and MgO: Fe films are between 3.4 and 3.55. Doping influences the optical quality [53].
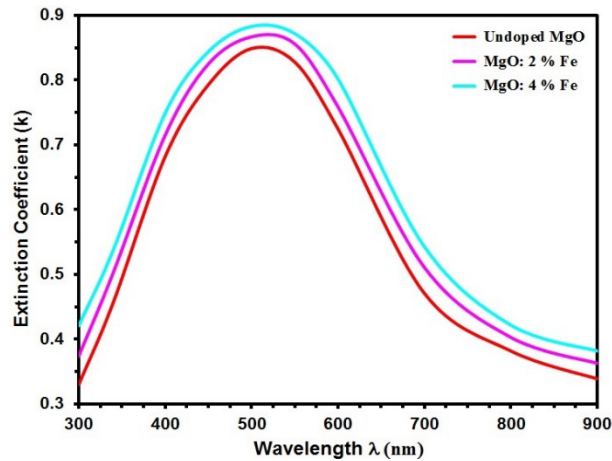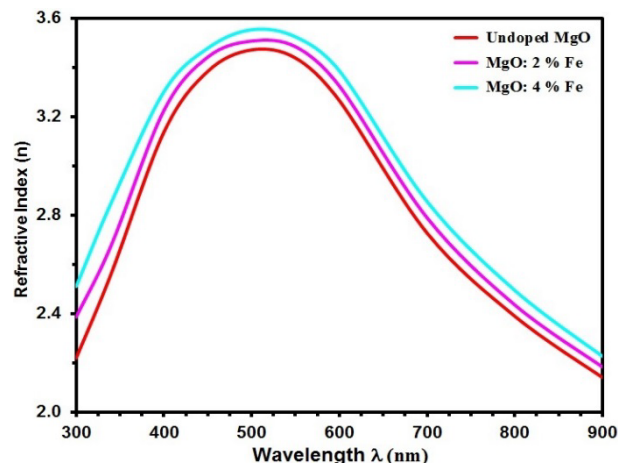
Fig. 8. k of grown films.

Fig. 9. n of the intended films.

In Fig. (10), the resistance via response time is depicted for films with doped and undoped thicknesses. The observed decrease in resistance for all samples upon introducing nitrogen dioxide gas into the chamber indicates that MgO behaves as a p-type semiconductor. This observation aligns with hall measurements, suggesting that oxidizing gases like NO_2 (a concentration of 250 ppm.) react with the film surface, capturing electrons from the conduction band. This process increases the number of holes (majority charge carriers in p-type semiconductors) in the conduction band, reducing film resistance [54]. The MgO:Fe doping at 4%wt concentration also demonstrated the highest resistance, suggesting the impact of doping on the semiconductor properties of the films [55].
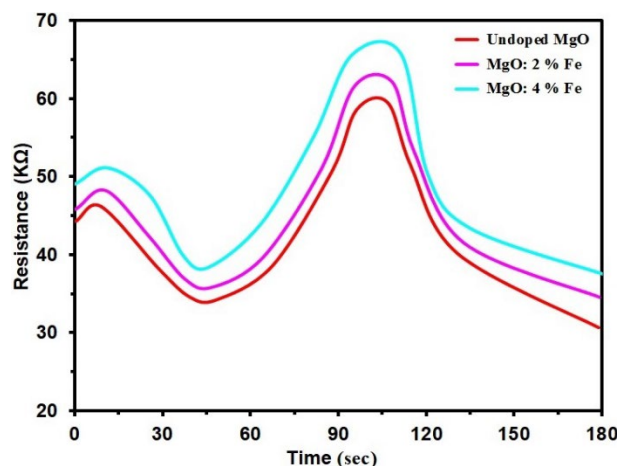
Fig. 10. Resistance as a function of operating time for MgO thin films with various Fe concentrations.

A film's sensitivity (S) is often gauged by the percentage alteration in resistance during gas exposure or defined as the ratio of its resistance in air to the steady-state value in the presence of gas. The sensor's response, or detection sensitivity, can be computed as [56, 57]:

$$Sensitivity = \frac{\Delta R}{R_g} = \left|\frac{R_g - R_a}{R_g}\right| \times 100\ \% \tag{9}$$

The sensitivity of MgO films, both pure and Fe-doped, to NO_2 exposure, is illustrated in Fig. 11. Sensitivity decreases with higher Fe concentrations, dropping from 49.9% to 4.5% (50 ppm), 52.2% to 9.8% (100 ppm), and 55.5% to 14.4% (150 ppm). This can be attributed to enhanced crystallinity and/or nano-crystalline size, increasing the gas reaction area and maintaining a homogenous surface. Additionally, heightened conductivity results from increased carrier concentration [58]. Fig. (11) indicates sensitivity rising with gas concentration from 50 to 150 ppm.
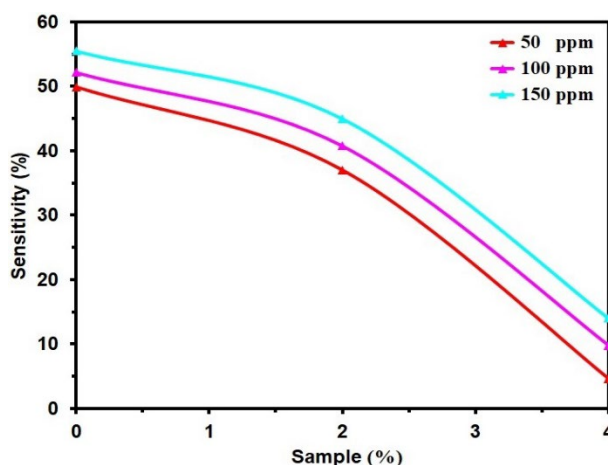

Fig. 11. Sensitivity (S) as a function of MgO thin films with various Fe concentrations.

4. Conclusion

The CSP method was employed to fabricate thin films of both pure MgO and MgO doped with Fe, resulting in cubic polycrystalline structures. As the Fe content increased from 0.0 to 4% wt, the crystallite size grew from 10.7 nm to 15.41 nm. AFM confirmed that the average particle size exhibited a uniform nanostructure. Introducing Fe doping led to a reduction in surface roughness from 7.83 to 5.17 nm. All the films displayed a transparency range of 60-70 %. Increasing concentration leads to enlarged grain size and surface roughening in SEM images, especially in the VIS region. A gradual increase in the absorption index in the VIS region was observed with an increase in Fe concentration. Doping induced a red shift in the bandgap, lowering it from 3.62 eV to 3.52 eV. Furthermore, films exhibited refractive indices in the visible part of the spectra ranging from 3.44 to 3.55. Gas sensitivity, indicated by resistance change, confirms MgO as p-type semiconductor. MgO:Fe at 4%wt shows the highest resistance. MgO films exhibit reduced NO_2 sensitivity with increased Fe concentration.

References

[1] P. Maiti, P. S. Das, M. Bhattacharya, S. Mukherjee, B. Saha, A. K. Mullick, and A. K. Mukhopadhyay, Mater. Res. Express, 4, 086405 (2017);https://doi.org/10.1088/2053-1591/aa8279
[2] H. Güney and D. Iskenderoğlu, Ceram. Int. 44, 7788 (2018); https://doi.org/10.1016/j.ceramint.2018.01.210
[3] S. H. Tamboli, R.B. Patil, S.V. Kamat, V. Puri, R. K. Puri, Journal of Alloys and Compounds, 477, 855-859 (2009); https://doi.org/10.1016/j.jallcom.2008.11.011
[4] M. Rezaei, M. Khajenoori, B. Nematollahi, Powder Technol. 205, 112 (2011); https://doi.org/10.1016/j.powtec.2010.09.001
[5] F. H. Jasim, H. R. Shakir, S. S. Chiad,N. F. Habubi, Y. H. Kadhi,, Jadan, M., Digest Journal of Nanomaterials and Biostructures, 18(4), 1385–1393 (2023); https://doi.org/10.15251/DJNB.2023.184.1385
[6] H. K. Yu, W. K. Kim, E. C. Park, J. S. Kim, B. W. Koo, Y. W. Kim, J. H. Ryu, J. L. Lee, J. Phys. Chem., C 115, 17910 (2011); https://doi.org/10.1021/jp205759s
[7] A. A. Abdul Razaq , F. H. Jasim , S. S. Chiad , F. A. Jasim, Z. S. A. Mosa , Y. H. Kadhimd, Journal of Ovonic Research, 20 (2), 131 – 141 (2024); https://doi.org/10.15251/JOR.2024.202.131
[8] F. A. Jasima , Z. S. A. Mosa, N. F. Habubi, Y. H. Kadhim, S. S. Chiad, Digest Journal of Nanomaterials and Biostructures, 18 (3), 1039–1049 (2023); https://doi.org/10.15251/DJNB.2023.183.1039
[9] S.Kaneko, T.Ito, M. Soga, Y.Motoizumi, M.Yasui, Y.Hirabayashi, T.Ozawa, M.Yoshimoto, Jpn. J. Appl. Phys., 52, 01AN02, (2013); doi: 10.7567/JJAP.52.01AN02
[10] G. Carta, N.El Habra, L. Crociani, G.Rossetto, P.Zanella, G.Paolucci, D. Barreca, E. Tondello, Chem. Vap. Depos., 13,185–189, (2007); doi: 10.1002/cvde.200606574
[11] V. Dhanasekaran, T. Mahalingam, J.-K. Rhee, J.P. Chu, Optik 124, 255–260 (2013); https://doi.org/10.1016/j.ijleo.2011.11.063
[12] P. Płóciennik, D. Guichaoua, A. Zawadzka, A. Korcala, J. Strzelecki, P. Trzaska, B. Sahraoui, Opt. Quantum Electron., 48, 277 (2016); doi: 10.1007/s11082-016-0536-8
[13] I.-C. Ho, Y. Xu, J. D. Mackenzie, J. Sol-Gel Sci. Technol., 9,295–301 (1997); doi: 10.1007/BF02437193
[14] R. Wahab, S. Ansari, M. Dar, Y.S. Kim, H.S. Shin, Mater. Sci. Forum, 2007,983–986 (2007); doi: 10.4028/www.scientific.net/MSF.558-559.983
[15] Y. W. Choi, J. Kim, Thin Solid Films, 460, 295–299 (2004); doi: 10.1016/j.tsf.2004.01.066

[16] F. Niu, B. H. Hoerman, B. W. Wessels, MRS Online Proc. Libr. 619,149–154 (2000); doi: 10.1557/PROC-619-149

[17] A. I. Popov, L. Shirmane, V. Pankratov, A. Lushchik, A. Kotlov, V. E. Serga, L. D. Kulikova, G. Chikvaidze, J. Zimmermann, Interactions with Materials and Atoms, 310 , 23-26 (2013); https://doi.org/10.1016/j.nimb.2013.05.017

[18] A.M.E. Raj, L.C. Nehru, M. Jayachandran, C. Sanjeeviraja, Cryst. Res. Technol, 42:867–875 (2007); doi: 10.1002/crat.200710918.

[19] Y. Li, H. Zhao, Z. Yang, J. Li, Y. Shi, Chemical Engineering Journal, 259, 680-689. (2015); DOI: 10.1016/j.cej.2014.07.032

[20] M. Tlili, N. Jebbari, W. Naffouti, N.T. Kamoun, Eur. Phys. J. Plus., 135, 1–12 (2020); doi: 10.1140/epjp/s13360-020-00706-z.

[21] A. Merazga, F. Al-Subai, A. M. Albaradi, A. Badawi, A. Y. Jaber, and A. A. B. Alghamdi, Mater. Sci. Semicon. Proc., 41, 114 (2016); https://doi.org/10.1016/j.mssp.2015.08.026

[22] D. Cáceres, I. Vergara, and R. González, J. Appl. Phys. 93, 4300 (2003); https://doi.org/10.1063/1.1558964

[23] Khadayeir, A. A., Hassan, E. S., Mubarak, T. H., Chiad, S.S., Habubi, N. F., Dawood, M.O., Al-Baidhany, I. A., Journal of Physics: Conference Series, 1294 (2) 022009(2019); https://doi.1088/1742-6596/1294/2/022009

[24] N. Y. Ahmed, B. A. Bader, M. Y. Slewa, N. F. Habubi, S. S. Chiad, NeuroQuantology, 18(6), 55-60 (2020); https://doi.org/10.1016/j.jlumin.2021.118221

[25] A. J. Ghazai, O. M. Abdulmunem, K. Y. Qader, S. S. Chiad, N. F. Habubi, AIP Conference Proceedings 2213 (1), 020101 (2020); https://doi.org/10.1063/5.0000158

[26] H. A. Hussin, R. S. Al-Hasnawy, R. I. Jasim, N. F. Habubi, S. S. Chiad, Journal of Green Engineering, 10(9), 7018-7028 (2020); https://doi.org/10.1088/1742-6596/1999/1/012063

[27] G. Carta, N. El Habra, L. Crociani, G. Rossetto, Pi. Zanella, A. Zanella, G. Paolucci, D. Barreca, and E. Tondello, Chem. Vapor. Depos. 13, 185 (2007); https://doi.org/10.1002/cvde.200606574

[28] S. S. Chiad, H. A. Noor, O. M. Abdulmunem, N. F. Habubi, M. Jadan, J. S. Addasi, Journal of Ovonic Research, 16 (1), 35-40 (2020). https://doi.org/10.15251/JOR.2020.161.35

[29] H. T. Salloom, E. H. Hadi, N. F. Habubi, S. S. Chiad, M. Jadan, J. S. Addasi, Digest Journal of Nanomaterials and Biostructures, 15 (4), 189-1195 (2020); https://doi.org/10.15251/DJNB.2020.154.1189

[30] N. N. Jandow, M. S. Othman, N. F.Habubi, S. S. Chiad, K. A. Mishjil, I. A. Al-Baidhany, Materials Research Express, 6 (11), (2020); https://doi.org/10.1088/2053-1591/ab4af8

[31] M. S. Othman, K. A. Mishjil, H. G. Rashid, S. S. Chiad, N. F. Habubi, I. A. Al-Baidhany, Journal of Materials Science: Materials in Electronics, 31(11), 9037-9043 (2020); https://doi.org/10.1007/s10854-020-03437-0

[32] E. S. Hassan, K. Y. Qader, E. H. Hadi, S. S. Chiad, N. F. Habubi, K. H. Abass, Nano Biomedicine and Engineering, 12(3), pp. 205-213 (2020); https://doi.org/10.5101/nbe.v12i3.p205-213

[33] E. H. Hadi, D. A. Sabur, S. S. Chiad, N. F. Habubi, K., Abass, Journal of Green Engineering, 10 (10), 8390-8400 (2020); https://doi.org/10.1063/5.0095169

[34] I. A. Kariper and F. M. Tezel, Ceram. Int. 45, 9219 (2019); https://doi.org/10.1016/j.ceramint.2019.01.267

[35] K. S. Sharba, A. S. Alkelaby, M. D. Sakhil, K. H. Abass, N. F. Habubi, S. S. Chiad, Enhancement of urbach energy and dispersion parameters of polyvinyl alcohol with Kaolin additive, NeuroQuantology, 18 (3), 66-73 (2020); https://doi.org/10.14704/NQ.2020.18.3.NQ20152

[36] M. D. Sakhil, Z. M. Shaban, K. S. Sharba, N. F. Habub, K. H. Abass, S. S. Chiad, A. S. Alkelaby, NeuroQuantology, 18 (5), 56-61 (2020); https://doi.org/10.14704/nq.2020.18.5.NQ20168

[37] O. M. Abdulmunem, A. M. Jabbar, S. K. Muhammad, M. O. Dawood, S. S. Chiad, N. F. Habubi, Journal of Physics: Conference Series,1660 (1), 012055 (2020); https://doi.org/ 10.1088/1742-6596/1660/1/012055

1106

[38] E. H. Hadi, M. A. Abbsa, A. A. Khadayeir, Z. M. Abood, N. F. Habubi, and S.S. Chiad, Journal of Physics: Conference Series, 1664 (1), 012069 (2020); https://doi.org/ 10.1088/1742-6596/1664/1/012069

[39] R. I. Jasim, E. H. Hadi, S. S. Chiad, N. F. Habubi, M. Jadan, J. S. Addasi, Journal of Ovonic Research, 19 (2), 187 – 196 (2023)..

[40] H.T. Salloom, R. I. Jasim, N. F. Habubi, S. S. Chiad, M. Jadan, J. S. Addasi, Chinese Physics, 30 (6), 068505 (2021); https://doi.org/ 10.10.1088/1674-1056/abd2a7

[41] K. Y. Qader, E. H. Hadi, N. F. Habubi, S. S. Chiad, M. Jadan, J. S. Addasi, International Journal of Thin Films Science and Technology, 10 (1), 41-44 (2021); https://doi.org/ 10.18576/ijtfst/100107

[42] R. S. Ali, M. K. Mohammed, A. A. Khadayeir, Z. M. Abood, N. F. Habubi and S. S. Chiad, Journal of Physics: Conference Series, 1664 (1), 012016 (2020); https://doi:10.1088/1742-6596/1664/1/012016

[43] A. S. Al Rawas, M. Y. Slewa, B. A. Bader, N. F. Habubi, S. S. Chiad, Journal of Green Engineering,10 (9), 7141-7153 (2020); https://doi.org/10.1021/acsami.1c00304

[44] R. S. Ali, H. S. Rasheed, N. F. Habubi, S.S. Chiad, Chalcogenide Letters,, 20 (1), 63–72 (2023; https://doi.org/10.15251/CL.2023.201.63

[45] K. Y. Qader, R. A. Ghazi, A. M. Jabbar, K. H. Abass, S. S. Chiad, Journal of Green Engineering, 10 (10), 7387-7398 (2020); https://doi.org/10.1016/j.jece.2020.104011

[46] A. Ghazai, K. Qader, N. F. Hbubi, S. S. Chiad, O. Abdulmunem, IOP Conference Series: Materials Science and Engineering, 870 (1), 012027 (2020); https://doi.org/ 10.1088/1757-899X/870/1/012027

[47] B. A. Bader, S. K. Muhammad, A. M. Jabbar, K. H. Abass, S. S. Chiad, N. F. Habubi, J. Nanostruct, 10(4): 744-750, (2020); https://doi.org/ 10.22052/JNS.2020.04.007

[48] R. S Ali, N. A. H. Al Aaraji, E. H. Hadi, N. F. Habubi, S. S. Chiad, Journal of Nanostructures, 10(4), 810–816 (2020); https://doi: 10.22052/jns.2020.04.014

[49] A. A. Khadayeir, R. I. Jasim, S. H. Jumaah, N. F, Habubi, S. S. Chiad, Journal of Physics: Conference Series,1664 (1) (2020); https://doi.org/10.1088/1742-6596/1664/1/012009

[50] S. S Chiad,, A. S. Alkelaby, K. S. Sharba,, Journal of Global Pharma Technology, 11 (7), 662-665, (2020); https://doi.org/10.1021/acscatal.1c01666

[51] Chiad, S.S., Noor, H.A., Abdulmunem, O.M., Habubi, N.F., Journal of Physics: Conference Series 1362(1), 012115 (2019); https://doi.org/10.1088/1742-6596/1362/1/012115

[52] S. K. Muhammad, M. O. Dawood, N. Y. Ahmed, E. S. Hassan, N. F. Habubi, S. S. Chiad, Journal of Physics: Conference Series, 1660 (1), 012057 (2020); https://doi.org/ 10.1088/1742-6596/1660/1/012057

[53] A. S. Alkelaby, K. H. Abass, T. H. Mubarak, N. F. , Habubi, S. S. Chiad, I. Al-Baidhany, Journal of Global Pharma Technology 11(4), 347-352 (2019).

[54] Khadayeir, A.A., Abass, K.H., Chiad, S.S., Mohammed, M.K., Habubi, N.F., Hameed, T.K., Al-Baidhany, I. A., Journal of Engineering and Applied Sciences 13(22), 9689-9692 (2018); https://doi.org/ 10.3923/jeasci.2018.9689.9692

[55] A. A. Khadayeir, E. S. Hassan, S. S. Chiad, N. F. Habubi, K. H. Abass, M. H. Rahid, T. H. Mubarak, M. O. Dawod, and I.A. Al-Baidhany, Journal of Physics: Conference Series 1234 (1), 012014, (2019); https://doi.10.88/1742-6596/1234/1/012014

[56] Hassan, E.S., Mubarak, T.H., Chiad, S.S., Habubi, N.F., Khadayeir, A.A., Dawood, M.O., Al-Baidhany, I. A. , Journal of Physics: Conference Series, 1294(2), 022008 (2019); https://doi.10.88/1742-6596/1294/2/022008

[57] M.O. Dawood, S.S. Chiad, A.J. Ghazai, N.F. Habubi, O.M. Abdulmunem, AIP Conference Proceedings 2213, 020102,(2020); https://doi.org/10.1063/5.0000136

[58] J. Jiu, K.I. Kurumada, M. Tanigaki, S. Yoshikawa, Mater. Lett. 58, 44–47 (2003); https://doi.org/10.1016/S0167-577X(03)00411-7